

AD-A248 446



IT DOCUMENTATION PAGE

Form Approved  
OMB No. 0700-0188

2

2b. DECLASSIFICATION/DOWNGRADING SCHEDULE UNCLASSIFIED		1b. RESTRICTIVE MARKINGS	
4. PERFORMING ORGANIZATION REPORT NUMBER(S)		3. DISTRIBUTION STATEMENTS OF REPORT This document has been approved for public release and sale; its distribution is unlimited.	
6a. NAME OF PERFORMING ORGANIZATION Dept. of Chemistry Cornell University	6b. OFFICE SYMBOL (if applicable)	7a. NAME OF MONITORING ORGANIZATION Office of Naval Research	
6c. ADDRESS (City, State, and ZIP Code) Dept. of Chemistry Cornell University Ithaca, NY 14853-1301		7b. ADDRESS (City, State, and ZIP Code) Chemistry Program 800 N. Quincy St. Alexandria, VA 22217	
8a. NAME OF FUNDING/SPONSORING ORGANIZATION Office of Naval Research	8b. OFFICE SYMBOL (if applicable)	9. PROCUREMENT INSTRUMENT IDENTIFICATION NUMBER N00014-91-J-1269	
8c. ADDRESS (City, State, and ZIP Code) Chemistry Program 800 N. Quincy St. Alexandria, VA 22217		10. SOURCE OF FUNDING NUMBERS	
		PROGRAM ELEMENT NO	PROJECT NO
		TASK NO	WORK UNIT ACCESSION NO.
11. TITLE (Include Security Classification) LiMoN <sub>2</sub> : The First Metallic Layered Nitride			
12. PERSONAL AUTHOR(S) S. H. Elder, Linda H. Doerrler, F. J. DiSalvo, J. B. Parise, D. Guyomard, J. M. Tarascon			
13a. TYPE OF REPORT Technical Rpt. #16	13b. TIME COVERED FROM 12/91 TO 11/94	14. DATE OF REPORT (Year, Month, Day) 92-April-2	15. PAGE COUNT
16. SUPPLEMENTARY NOTATION Submitted to: Chemistry of Materials			
17. COSATI CODES		18. SUBJECT TERMS (Continue on reverse if necessary and identify by block number)	
FIELD	GROUP	SUB-GROUP	
		Solid State Nitrides Li batteries	
		Crystal Structure Magnetic & Electrical Properties	
19. ABSTRACT (Continue on reverse if necessary and identify by block number) We report the first example of a layered ternary lithium nitride in which the lithium can be deintercalated and reintercalated. This ternary nitride, LiMoN <sub>2</sub> , has been synthesized by the reaction of two different precursors, Li <sub>2</sub> Mo(N <sup>t</sup> Bu) <sub>4</sub> and Li <sub>2</sub> MoO <sub>4</sub> , with ammonia gas. The structure was refined using a combination of X-ray and neutron powder diffraction data in the space group R3 and the lattice parameters are (Å) a=2.8672(3) and c=15.813(3) which were obtained from the neutron data. The ideal structure consists of MoN <sub>2</sub> layers with Mo in trigonal prismatic holes and Li in octahedral holes between the MoN <sub>2</sub> layers. The diffraction studies indicate the presence of cation anti-site defects; the structure is best described as  (CONTINUED ON REVERSE)			
20. DISTRIBUTION/AVAILABILITY OF ABSTRACT <input checked="" type="checkbox"/> UNCLASSIFIED/UNLIMITED <input checked="" type="checkbox"/> SAME AS RPT <input type="checkbox"/> DTIC USERS		21. ABSTRACT SECURITY CLASSIFICATION Unclassified	
22a. NAME OF RESPONSIBLE INDIVIDUAL Dr. John Pazik		22b. TELEPHONE (Include Area Code) 202-696-4409	22c. OFFICE SYMBOL

$(\text{Li}_{0.84}\text{Mo}_{0.16})_{\text{oct}}(\text{Mo}_{0.84}\text{Li}_{0.16})_{\text{tp}}\text{N}_2$ .  $\text{LiMoN}_2$  is metallic and Pauliparamagnetic with  $\chi_0 = 0.59 \times 10^{-6} \text{ emu g}^{-1}$ . We have employed a variety of different oxidizing agents for the deintercalation of the lithium from  $\text{LiMoN}_2$  and have been able to deintercalate up to 64% of the lithium. This deintercalated species can be reintercalated with n-butyllithium (in hexane) at room temperature. Electrochemical studies show a large hysteresis in charge-discharge cycles.

OFFICE OF NAVAL RESEARCH

Grant or Contract N00014-91-J-1269

R&T Code 4134037

Technical Report No. 16

$\text{LiMoN}_2$ : the First Metallic Layered Nitride

by

S. H. Elder, L. H. Doerrler, F. J. DiSalvo  
J. B. Parise, D. Guyomard and J. M. Tarascon

Submitted to  
Chemistry of Materials

Cornell University  
Department of Chemistry  
Ithaca, NY 14853

April 2, 1992

Accession For	
NTIS CR&I	<input checked="" type="checkbox"/>
DTIC TAB	<input type="checkbox"/>
Unannounced	<input type="checkbox"/>
Justification	
By _____	
Distribution/	
Availability Codes	
Dist	Availability or Special
A-1	

Reproduction in whole or in part is permitted for any purpose  
of the United States Government

This document has been approved for public release  
and sale; its distribution is unlimited

92 4 10 105

92-09373



# **LiMoN<sub>2</sub>: The First Metallic Layered Nitride**

**S. H. Elder, Linda H. Doerrler and F. J. DiSalvo\***

Department of Chemistry, Baker Laboratory  
Cornell University, Ithaca, New York 14853-1301

**J. B. Parise**

Mineral Physics Institute, State University  
of New York at Stony Brook, Stony Brook, NY 11794

**D. Guyomard and J. M. Tarascon**

Bell Communications Research, 311 Newman Springs Rd., Redbank, NJ 07701

**\*to whom correspondence should be addressed**

## Introduction

Binary nitrides are known for most metals of the periodic table with the exception of the alkali metals (excluding Li) and the late 4d and 5d elements. However, ternary nitrides are not well studied, except for the well known lithium rich transition metal nitrides.<sup>1-3</sup> Many lithium rich ternary nitrides have been synthesized; however, the synthetic route has been similar in all cases: growth from a lithium nitride flux. Likewise, the structures show great similarities; almost all are superstructures of anti-fluorite.

Recent work has produced numerous alkaline and alkaline earth transition metal nitrides with interesting chemical, structural and physical properties:  $MNiN$  ( $M = Ca, Sr$  or  $Ba$ ),<sup>4,5</sup>  $Ca_3MN$  ( $M = P, As, Sb, Bi, Ge, Sn, Pb$ ),<sup>6</sup>  $MTaN_2$  ( $M = Na, K, Rb, Cs$ ),<sup>7</sup>  $Ca_3CrN_3$ ,<sup>8</sup>  $Ca_6MN_5$  ( $M = Ga$  and  $Fe$ ),<sup>9</sup>  $Ba_3MN_4$  ( $M = Mo$  and  $W$ ),<sup>10</sup>  $Ba_3FeN_3$ <sup>11</sup> and  $M_2LiFe_2N_3$  ( $M = Sr$  and  $Ba$ ).<sup>12</sup>

The chemistry and properties of the lithium intercalated dichalcogenide layered compounds  $LiMX_2$  ( $X = S, Se$ ;  $M = IVb, Vb, VIb$  transition metals) have been known and studied for over 25 years.<sup>13,14</sup> Long term interest in these materials is due in part to their potential use in recyclable lithium batteries<sup>15</sup> and as catalysts.

Since nitrides have small free energies of formation due in part to the strong triple bond in dinitrogen, the synthesis of such phases at the high temperatures necessary to obtain reasonable solid state diffusion is often precluded because the phases are only stable at lower temperatures. Therefore, we are developing lower temperature synthesis strategies based

on the reaction of suitable mixed metal precursors with ammonia gas to produce ternary nitrides. Herein we report the synthesis of a new metallic, layered nitride,  $\text{LiMoN}_2$ , from two such precursors, and discuss its chemical and physical properties.

## Experimental Section

**Starting Materials.** The precursor  $\text{Li}_2\text{Mo}(\text{N}^t\text{Bu})_4$  was prepared according to published methods.<sup>16</sup> Lithium molybdate was prepared by heating a 1:1 mixture of  $\text{Li}_2\text{CO}_3$  (99.99% metals purity) and  $\text{MoO}_3$  (ACS grade) at  $650^\circ\text{C}$  for approximately 18h in air;  $\text{Li}_2\text{MoO}_4$  was identified as a pure product by X-ray powder diffraction methods. All manipulations of  $\text{Li}_2\text{Mo}(\text{N}^t\text{Bu})_4$  and  $\text{LiMoN}_2$  were carried out in an argon filled box or on a vacuum/argon manifold due to their known or anticipated air sensitivity.

**Synthesis of  $\text{LiMoN}_2$ .** The title compound was first synthesized by decomposing  $\text{Li}_2\text{Mo}(\text{N}^t\text{Bu})_4$  (in an alumina boat) under flowing ammonia gas at  $650^\circ\text{C}$  in a nitriding apparatus.<sup>17</sup> The product formed was a free flowing, black powder that appeared graphitic-like on grinding. The X-ray powder pattern consisted of a small number of intense peaks and several weak peaks. The intense peaks could be indexed by assuming a hexagonal unit cell with  $a = 2.868 \text{ \AA}$  and  $c = 15.787 \text{ \AA}$ , with systematic zeroes that suggest rhombohedral symmetry. Since no binary Mo-N phases have these lattice parameters, it was clear that a ternary phase had formed. Due to the graphitic nature of the compound, we also suspected that the structure

was layered.

Since  $\text{LiVS}_2$  can be prepared by heating  $\text{Li}_2\text{CO}_3$  and  $\text{V}_2\text{O}_5$  in flowing  $\text{H}_2\text{S}$  gas at  $750^\circ\text{C}$ ,<sup>18</sup> it seemed possible that a ternary nitride phase could be obtained by the reaction of  $\text{Li}_2\text{MoO}_4$  with ammonia gas. We found that the same well crystallized black powder, as identified by X-ray diffraction, could be prepared by exposing a melt of  $\text{Li}_2\text{MoO}_4$  (in an alumina boat) to flowing ammonia gas at  $710^\circ\text{C}$  for 16h in the nitriding apparatus (large scale reactions may require grinding and reheating in flowing ammonia gas for complete reaction). Again, weak peaks could be seen in the X-ray diffraction pattern. In this latter case, the weak peaks could be entirely accounted for by the presence of lithium oxide. Since the preparation of  $\text{Li}_2\text{Mo}(\text{N}^t\text{Bu})_4$  is relatively time consuming, we now exclusively synthesize the ternary nitride from  $\text{Li}_2\text{MoO}_4$ .

The thermal decomposition of  $\text{Li}_2\text{MoO}_4$  in flowing ammonia gas occurs in at least a few distinct steps. When  $\text{Li}_2\text{MoO}_4(\text{s})$  was heated in ammonia, it turned black by approximately  $450^\circ\text{C}$ . Upon grinding, the powder was gray and the only crystalline phase detected by X-ray powder diffraction was  $\text{Li}_2\text{MoO}_4$ . This was indicative that a black, amorphous coat had formed on the  $\text{Li}_2\text{MoO}_4$  particles. At  $500^\circ\text{C}$  the powder was black when ground and one crystalline phase,  $\text{Li}_4\text{MoO}_5$ , was detected by X-ray diffraction. A second phase that must be present for mass balance remained amorphous. Within the range of  $650 - 710^\circ\text{C}$ , the ternary nitride and  $\text{Li}_2\text{O}$  were the only phases observed as determined by X-ray diffraction and mass loss from the reaction. Finally, by  $850^\circ\text{C}$  the ternary nitride decomposed and the  $\text{Li}_2\text{O}$  sublimed leaving only  $\gamma\text{-Mo}_2\text{N}$  in the reaction vessel as determined by X-ray diffraction and mass loss.

When a melt of  $\text{Li}_2\text{MoO}_4$  (mp = 705° C) was exposed to ammonia at 710° C, a homogeneous, black powder quickly formed; upon heating for 20min at 710° C and then quenching, only  $\text{Li}_4\text{MoO}_5$  was detected by X-ray diffraction. However, when the heating of this powder was continued for 12h it was converted completely to the ternary phase and  $\text{Li}_2\text{O}$ .

The thermal stability of the ternary phase seems to lie in a fairly narrow temperature range. When reaction temperatures are below the melting point of  $\text{Li}_2\text{MoO}_4$  (for example at 675°C), the kinetics of the reaction are slowed dramatically yielding incomplete ammonolysis of the oxide. However, at temperatures greater than ~735°C partial decomposition to  $\gamma\text{-Mo}_2\text{N}$  is evident by both X-ray and neutron powder diffraction, as well as an increased concentration of anti-site defects in the ternary phase (vide infra). An increased time of heating appears to increase the degree of decomposition.

In order to determine the composition, structure and properties of this new ternary nitride, it was necessary to remove the lithium oxide. Although the lithium oxide was readily removed by washing with water, the title compound appeared to be somewhat reactive towards water and/or aqueous base. Washing the nitride with water lead to a mass loss which was too great for the loss of lithium oxide exclusively; also some ammonia gas was produced as evident by its acrid odor. Washing with dried ethanol also removed the lithium oxide, but again it appeared to allow some small side reaction, as determined by new peaks in the X-ray diffraction pattern and mass loss, although the loss is much less than with water. We have not pursued this ethanol reaction further.

We found that the lithium oxide could be most successfully removed by condensing ammonia (approximately 10mL  $\text{NH}_3$  / 0.15g nitride), predried

over sodium, onto a mixture of ammonium chloride and the nitriding reaction product;<sup>19</sup> 2.2 moles of ammonium chloride were used for every mole of lithium oxide present. The products of this reaction are lithium chloride, ammonia and water. This mixture was periodically stirred for 2h at approximately -35° C in an H-cell.<sup>19</sup> The ammonia was decanted off and the nitride was washed several times with fresh ammonia to remove the less soluble lithium chloride and any remaining ammonium chloride. The X-ray powder pattern was clean, no reactions with the ammonia or side products were evident. The presence of the small amount of water from this reaction did not seem to cause side reactions perhaps due to two factors: the reaction takes place below 0° C leading to slow kinetics, and the small amount of water produced should be strongly coordinated to the lithium cations present.

**Analysis.** Solutions of the ternary phases were prepared by dissolution of the solids in aqua regia (this requires several hours at room temperature);  $\text{Li}_2\text{MoO}_4$ , dissolved in a like manner, was used as a standard. Metals analysis was done on solutions using Plasma Emission Spectroscopy (PES). The molybdenum line ( $\lambda = 202.2\text{nm}$ ) was analyzed on a Jarrel-Ash I.C.A.P 61 update spectrometer and the lithium line ( $\lambda = 670.8\text{nm}$ ) on a model 82-000 modified Ebert Mount spectrometer. The Li:Mo ratio ranged from 0.95 - 0.97:1.00 leading to a stoichiometry (expected accuracy of  $\pm 2\%$ ) of  $\text{Li}_{0.96}\text{MoN}_2$ ; we refer to this hereafter as  $\text{LiMoN}_2$ . Metals analysis (PES) indicated the stoichiometry (or the ratio of the metals) of the parent compound deintercalated (see section on chemical properties) with DDQ and  $\text{NOBF}_4$  to be  $\text{Li}_{0.44}\text{MoN}_2$  and  $\text{Li}_{0.36}\text{MoN}_2$  respectively

(assumed nitrogen content).

Since  $\text{LiMoN}_2$  will not dissolve in  $\text{H}_3\text{PO}_4$ <sup>20</sup> or  $\text{H}_2\text{SO}_4$  (Kjeldahl method), the nitrogen content could not be directly determined from evolved ammonia. Using the modified Dumas method,<sup>21</sup> we obtained 76% of the expected  $\text{N}_2$ . However, the sample could not be completely reacted with carbon dioxide even at  $1000^\circ\text{C}$  as was evident by the black color of the sample after the reaction (complete reaction would leave a white oxide or carbonate powder). Consequently, this measurement can only put a lower limit on the N:Mo ratio of 1.5. However, by mass difference from the PES data, the N:Mo ratio is 2.2:1 ( $\pm 15\%$ ).

The weight loss upon reaction of  $\text{Li}_2\text{MoO}_4$  with ammonia was consistent with the formation of one half mole lithium oxide and one mole of  $\text{LiMoN}_2$  for each mole of  $\text{Li}_2\text{MoO}_4$ . Also, the measured density<sup>22</sup> of  $\text{LiMoN}_2$  powder was  $5.72 \text{ g cm}^{-3}$  ( $\pm 2\%$ ) compared with the calculated density of  $5.79 \text{ g cm}^{-3}$  (see section on structure).

Although we have been unable to make a direct analysis for nitrogen, thermal gravimetric analysis (TGA) does give an upper limit of oxide contamination. Figure 1 shows the mass change upon heating  $\text{LiMoN}_2$  in air.

### Figure 1

The mass gain of 21.08% is close to the theoretical value of 21.38% for the decomposition of  $\text{LiMoN}_2$  to  $1/2 \text{ Li}_2\text{O}$  and  $\text{MoO}_3$  or corresponding ternary oxides; this places an upper limit of about 10% oxygen content in the nitride (i.e.  $\text{LiMoN}_{2-x}\text{O}_x$ ;  $x < 0.2$ ) Coupled with the fact that the  $\text{LiMoN}_2$  initially

synthesized from  $\text{Li}_2\text{Mo}(\text{N}^t\text{Bu})_4$  had lattice parameters identical to that of the  $\text{LiMoN}_2$  prepared from the oxide, leads us to believe that the oxygen "contamination" is much smaller than 10%.

### Structure Determination.

**X-ray Diffraction.** Initial X-ray powder diffraction data<sup>4</sup> were collected with a Scintag XDS 2000 diffractometer using  $\text{CuK}\alpha$  radiation.

The X-ray powder pattern (Fig. 2) was easily indexed on a hexagonal unit

### Figure 2

cell with  $a = 2.868 \text{ \AA}$  and  $c = 15.787 \text{ \AA}$ . However, the systematic absences in the  $(10l)$  and the  $(00l)$  lines show that the correct space group is rhombohedral. Assuming that the structure consists of  $\text{MoN}_2$  layers with close-packed layers of nitrogen sandwiching a layer of molybdenum and octahedral coordination for lithium (as is found in the layered sulfides), we were limited to two rhombohedral space groups:  $R\text{-}3m$  (no. 166) and  $R3$  (no. 146). The only difference between these two space groups is the nitrogen coordination about the molybdenum;  $R\text{-}3m$  places the molybdenum in an octahedral hole while  $R3$  places it in a trigonal prismatic one. The assumed atomic positions in both space groups are listed in Table I. Table II lists the measured intensities and d-spacings from the X-ray powder pattern, as well as the calculated<sup>23</sup> intensities for the  $R\text{-}3m$  and  $R3$  structures.

**Table I & II**

There are some significant differences between the measured and the calculated intensities in either of the space groups; this is due in part to the preferred orientation that occurs when the graphite-like powder is packed into the X-ray sample holder. Even though the relative intensities of the (00 $l$ ) reflections are not affected by preferred orientation, they show considerable variance with the calculated intensities, especially the 006 and 009 lines. This was the first indication that some molybdenum may be located on lithium sites and vice versa.<sup>24</sup> Since X-ray powder diffraction is not sensitive for the detection of light atoms such as nitrogen and lithium, we collected neutron powder diffraction data which does not suffer from the sensitivity problems just mentioned.

**Neutron Diffraction.** A 6g sample of LiMoN<sub>2</sub> (a different sample than was used in the X-ray study) was loosely packed into a 1.5cm diameter vanadium can in an argon filled dry box. An aluminum cap was secured to the top with epoxy to prevent air exposure. The Li<sub>2</sub>O was not washed out because of the difficulty in handling such large volumes of liquid ammonia; hence this sample also contained about 0.5g of Li<sub>2</sub>O.

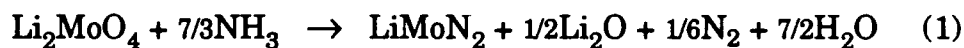
Neutron diffraction measurements on the sample were performed on a triple axis diffractometer at the H4S station of the Brookhaven High Flux Beam Reactor. The instrument configuration consisted of a pyrolytic graphite monochromator and analyzer, in the (002) and (004) settings respectively, along with collimator of 20' in-pile, 40' monochromator-sample, 40' sample-analyzer and 20' analyzer-detector. The higher order harmonics were eliminated with a pyrolytic graphite filter. The

wavelength was calibrated using  $\text{CeO}_2$  ( $a = 5.4113\text{\AA}$ ) and its value was  $1.3585\text{\AA}$ .

The pattern, shown in Figure 3, was collected in  $0.1^\circ$  steps in  $2\theta$  from 5

**Fig. 3**

to  $130^\circ$ . Inspection of the powder pattern data showed the presence of  $\text{Li}_2\text{O}$  as expected. Subsequent two phase refinement<sup>25</sup> suggested these components were in the molar ratio of 2:1, in agreement with the stoichiometry of the reaction



In addition to the  $\text{Li}_2\text{O}$  peaks expected for the described synthetic procedure, some weak peaks, less than 1% of the strongest peak in the pattern, occurred near 33, 38, 52 and 56 degrees  $2\theta$ . These were presumed to arise from an unknown impurity (perhaps  $\gamma\text{-Mo}_2\text{N}$ ) and these regions were not refined.

A series of preliminary refinements indicated that molybdenum was in trigonal prismatic coordination with nitrogen rather than octahedral, therefore further structure analysis was limited to space group  $R\bar{3}$ . Locating the lithium proved to be problematic. No peaks could be discerned in the Fourier difference maps that were calculated on the basis of the partial structure model and intensities extracted from the neutron diffraction pattern.

A refinement of the occupancy factor for the molybdenum suggested the reason for the difficulty in locating the lithium site. Assuming the site to be

occupied exclusively by molybdenum, its refined occupancy was 0.8 rather than 1.0. Since the stoichiometry  $\text{LiMoN}_2$  is consistent with the chemistry of this material and the relative proportions of  $\text{Li}_2\text{O}$  and  $\text{LiMoN}_2$  refined to 35% and 65% respectively, as expected, we assumed that there must be mixing between the lithium and molybdenum metal layers. As such, any deficiency in the molybdenum site should be coupled with a replacement of an equivalent of lithium in the lithium site by the molybdenum. The composition of the trigonal prismatic site can be easily estimated by 1) assuming the site to be fully occupied and 2) from the apparent scattering length observed for the site, presuming it to contain only molybdenum. Simultaneous solution of the equations suggested the compositions of the trigonal prismatic site and the as yet undisclosed lithiated site were  $(\text{Mo}_{0.84}\text{Li}_{0.16})$  and  $(\text{Li}_{0.84}\text{Mo}_{0.16})$  respectively. The total scattering expected from the latter site is then  $(0.84b_{\text{Li}} + 0.16b_{\text{Mo}} = -0.07)$ , where the b's refer to the scattering lengths of the elements occupying this site at random within the structure. This small value is consistent with the lack of peaks in the Fourier difference map.

The expected advantage neutron diffraction has over X-ray diffraction in this case is the large scattering difference between trigonal prismatic and octahedral coordination, and the inter-layer cations. This latter advantage has largely been negated by the anti-site defects. However, the presence of molybdenum in the lithium sites suggests favorable conditions for X-ray scattering. At  $\sin\theta/\lambda = 0.0$  the scattering expected for each lithium rich site is about  $0.84f_{\text{Li}} + 0.16f_{\text{Mo}} = 9.2$  electrons.

**Synchrotron X-ray Diffraction.** We collected a second set of X-ray data, shown in Figure 4, on a sample of  $\text{LiMoN}_2$  mounted in a 0.5mm capillary

**Fig. 4**

at a  $\lambda=1.2981\text{\AA}$  to obtain more quantitative information. This technique was used to correct for the preferred orientation expected in the powder diffraction for this layered material. Using the parameters obtained for the structure model derived from the neutron data, a Fourier difference map was calculated based on the X-ray data. This revealed a peak of height 5 electrons/ $\text{\AA}^3$  in the octahedral site between the  $\text{MoN}_2$  layers. This was estimated to correspond to 0.12Mo. Inclusion of this site lowered the profile discrepancy from 0.297 to 0.260. Inclusion of this same amount of scattering at the tetrahedral site (0,0,1/2) raised the discrepancy to 0.341.

The unique information offered by the X-ray and neutron experiments were combined in a refinement using both the X-ray and neutron powder diffraction data. Since these two sets of data were collected at different temperatures, three phases were used in the refinement. The first two of these were  $\text{LiMoN}_2$ . One phase for the X-ray data and one for the neutron data; the positional and thermal parameters for the two phases were constrained to be equal. Although the difference in the temperatures at which the two data sets were collected was small, 10K, this caused a measurable difference in the  $c$  cell parameter (see Table III). The third phase defined was  $\text{Li}_2\text{O}$ , a significant component of the sample used in the data collection. Both data sets were corrected for the effects of absorption (for X-ray case personal communication with J. Hriljac and for the neutron case A. W. Hewat, *Acta. Cryst.* **A35**, 248 (1979) as implemented in GSAS).

The model was refined with lithium/molybdenum mixed in the trigonal prismatic site and the inter-layer octahedral site. The refinement was

constrained such that the formula was maintained,  $\text{LiMoN}_2$ , and all sites were presumed to be fully occupied. The final refinement employed independent isotropic thermal parameters for all sites. The  $z$  parameter of the molybdenum site was fixed at zero in order to define the origin along the  $c$  axis.

We attempted to refine the neutron diffraction data in space groups that allowed the lithium to be placed in tetrahedral holes, molybdenum in octahedral holes (in the molybdenum rich layer) and combinations of these arrangements, but these refinements lead to structures that contained unreasonable metal-nitrogen bond lengths (much shorter than the expected:  $\text{Li-N} \sim 2.0 \text{ \AA}$  and  $\text{Mo-N} \sim 2.0 \text{ \AA}$ ),<sup>26,10</sup> and the fit between experimental and calculated data was not good.

The comparatively large thermal parameters for the lithium site may indicate some positional disorder for the lithium and molybdenum. The resulting structure and structural data from the refinement are displayed in Figure 5 and Tables III & IV

#### **Fig. 5, Tables III&IV**

We have observed in X-ray powder diffraction experiments that when  $\text{LiMoN}_2$  is reheated in ammonia gas the 006 line intensity increases by as much as 15%, indicating that the anti-site defect concentration or the disorder is increasing. We also considered the possibility that the structure may at least partially order at a lower temperature. A sample of  $\text{LiMoN}_2$ , containing 16% anti-site defects, was sealed in an evacuated quartz tube and annealed at  $300^\circ\text{C}$  for 34 days. An X-ray pattern of the resulting black

powder showed no visible decomposition and the relative intensities of the 003 and 006 reflections remained the same, indicating that the anti-site defect concentration was unaffected.

**Magnetic Susceptibility.** The magnetic susceptibility was measured from 4.2 K to 300 K on a previously calibrated<sup>27</sup> Faraday balance; the sample was sealed in a thin-walled Suprasil quartz tube under a partial pressure of helium. The room temperature susceptibility exhibited some magnetic field dependence indicative of a small amount of ferromagnetic impurity. The signal from the ferromagnetic impurity was subtracted by the method of Owen and Honda<sup>28</sup> and the corrected data are shown in Figure 6.

### Figure 6

The Curie tail at low temperature (the increase in  $\chi$  as T is lowered) can be attributed to a small amount of paramagnetic impurity. We fit the data to  $\chi_g = \chi_0 + C_g / (T+\theta)$  by a least squares method over a temperature range of 4.2 - 300 K. We obtained  $C_g = 1.15 \times 10^{-5} \text{ emu g}^{-1}$ ,  $\theta = 0$  and  $\chi_0 = 0.59 \times 10^{-6} \text{ emu g}^{-1}$  ( $\pm 2\%$ ); with a mean square deviation of data to the fit of 0.6%. This value of  $\chi_0$  is in the range of observed values for metallic transition metal compounds. The magnitude of  $C_g$  is consistent with  $\sim 0.04$  atomic percent iron (assuming  $g = 2$ ,  $S = 2$ ) impurity concentration. Although we have not directly measured impurity levels, iron is the most common paramagnetic impurity in solids and the calculated impurity level is consistent with the purity of the starting materials.

**Electrical Properties.** A simple two-point resistance measurement of  $\text{LiMoN}_2$  was made by pressing a sample of the powder (2.3mm thick, 2.6mm diameter) between two metal rods in an insulating alumina cylinder. The resistance of the pellet was less than  $0.01 \Omega$  (the lower limit of the measurement) greater than that measured when no powder was present between the rods; this lead to a calculated resistivity at room temperature of less than or equal to  $2 \times 10^{-3} \Omega \cdot \text{cm}$ . One major limitation of the two probe method is that it may be dominated by particle - particle contact resistance. Consequently, we can presently only give an upper limit of resistivity. Attempts to make sintered pellets for four probe resistivity measurements were unsuccessful due to the fragile nature of the pressed pellets.

**Chemical Properties.** Lithium can generally be intercalated into or deintercalated from layered structures; hence we felt this compound would be amenable to such reactions.

Several different oxidizing agents to remove lithium from  $\text{LiMoN}_2$  were investigated, including:  $\text{I}_2$ ,  $\text{Br}_2$ , DDQ (2,3-dichloro-5,6-dicyanobenzoquinone),  $\text{NOBF}_4$  and  $\text{NO}_2\text{BF}_4$ . The potentials of these oxidizing agents (in acetonitrile) versus a standard hydrogen electrode are shown in Figure 7.<sup>29</sup> The expected reactions, if all lithium were removed, are, for example:

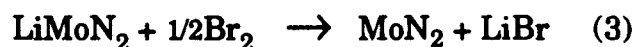
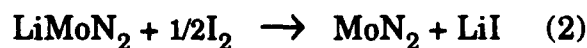




### Figure 7

In each case the product salts are soluble in acetonitrile, while the  $\text{MoN}_2$  and  $\text{LiMoN}_2$  are insoluble.

The general procedure was to reflux approximately 150mg of the nitride with a two-fold excess of the oxidizing agent dissolved in 50mL of dry (stirred over powdered 3Å sieves for at least 24h) acetonitrile for 1-2d. The mixture was filtered, washed with fresh acetonitrile and dried in the glovebox under vacuum. The extent of both deintercalation and side reaction was determined by X-ray powder diffraction, mass loss and PES analysis (see section on analysis).

No decolorization of the iodine (0.1M in acetonitrile) solution was observed when one equivalent of iodine was refluxed with the nitride. Furthermore, there was little or no lithium iodide formation (no mass change of the black  $\text{LiMoN}_2$  powder), and there were no changes in the X-ray powder diffraction pattern. We concluded that iodine was not a strong enough oxidizing agent to remove more than perhaps a few percent of the lithium.

The oxidizing power of the remaining agents was strong enough for at least partial deintercalation. When the first 0.1-0.2 equivalents of bromine solution (0.1M in acetonitrile) were added, decolorization of the solution was observed indicating deintercalation. However, when more than 0.2 equivalents of bromine were added, the solution became yellow indicating some decomposition of the  $\text{LiMoN}_2$ . The resulting X-ray powder pattern

showed some broadening of the peaks indicating that a small fraction of lithium had indeed been removed.

In the case of  $\text{NOBF}_4$  and  $\text{NO}_2\text{BF}_4$  the evolution of gas ( $\text{NO}$  and  $\text{NO}_2$ ) was observed which was indicative of reaction. However, there was a reasonable amount of decomposition of the nitride with the use of  $\text{NOBF}_4$  and  $\text{NO}_2\text{BF}_4$ . This was indicated by a yellow or brown filtrate after refluxing and washing the nitride, and a mass loss that was too great for just the removal of one equivalent of lithium from  $\text{LiMoN}_2$ . The products of decomposition have not been studied. The evolved  $\text{NO}(\text{g})$  and  $\text{NO}_2(\text{g})$  also appear to react with the nitride. If the evolved gas was not rapidly removed during the refluxing process, the resulting deintercalated species could not be reintercalated with n-butyllithium. It was likely that a pacifying coating had formed on the particles due to these oxidizing gases. When the gases were swept away by bubbling argon gas through the solution at  $\sim 0.5$  cc/s, the deintercalated nitride could be reintercalated with n-butyllithium (in hexane) at room temperature as was indicated by a shift of the lines in the X-ray diffraction pattern back to the original positions observed in  $\text{LiMoN}_2$ .

Reaction with DDQ produced a deep reddish-orange solution which was consistent with the formation of the  $\text{Li}^+\text{DDQ}^-$  salt. The mass loss was consistent with little or no side reaction. In all the above cases, significant shifts to smaller d-spacings for the (00l) lines were observed in the X-ray powder diffraction pattern. This is the expected result since this set of lines is most influenced by a change in the lithium content in layered compounds.

The X-ray powder pattern of the most lithium deficient phase obtained,  $\text{Li}_{0.36}\text{MoN}_2$ , along with that for  $\text{LiMoN}_2$ , is displayed in Figure 8; the lattice

constants for  $\text{Li}_{0.36}\text{MoN}_2$  were  $a = 2.862 \text{ \AA}$  and  $c = 15.529 \text{ \AA}$ . Several small peaks, indicative of the presence of a second phase, appear when the average lithium content is below  $\sim 0.5 \text{ Li/Mo}$ . Table V lists the d-spacings observed in both  $\text{LiMoN}_2$  and  $\text{Li}_{0.36}\text{MoN}_2$ .

### Figure 8 & Table V

We have been unsuccessful in removing all the lithium with any of the reagents.

**Electrochemistry.** To better understand the behavior of  $\text{LiMoN}_2$  with respect to lithium intercalation, we have performed electrochemical measurements using Swagelock test cells<sup>30</sup> assembled in a helium filled dry box. The positive electrode was a pressed pellet which consisted of 10mg  $\text{LiMoN}_2$ , 9% carbon black and 1% EPDM (ethylenepropylenediene monomer - used as a binder); the negative electrode was a lithium disc. The electrodes were separated by a porous glass filter paper soaked in an electrolyte that consisted of a 1M solution of  $\text{LiClO}_4$  in a 50-50 ethylene carbonate (EC)-diethoxyethane (DEE) mixture. The electrochemical cells were studied in both galvanostatic and potentiostatic modes using a Mac Pile system.<sup>31</sup> By monitoring the voltage of a  $\text{LiMoN}_2/\text{Li}$  cell while it was charged and discharged at constant current (galvanostatic mode), we observed a large voltage polarization (voltage difference between open circuit and closed circuit curves) suggesting that the kinetics of the lithium deintercalation process in  $\text{LiMoN}_2$  is very slow. Because of this early finding, we have mainly used the potentiostatic mode to further study this

system.

The voltage-composition curves are shown for two electrochemical cells in Figures 9 and 10. Cell 1 (Fig. 9) has been charged at a scan rate of 2mV/hr up to 4.2V and then discharged to 2.7V, while cell 2 (Fig. 10) has

### Fig. 9 & 10

been charged to 4.1V at a higher scan rate of 10mV/hr and then cycled between 4.1V and 0.02V for one cycle.

In cell 1, we note on charge the presence of two pseudo-plateaus located at an average voltage of 3.73V and 4.07V corresponding to a capacity of about 100 and 75 mAh/g respectively. On the discharge following the second plateau, an oxidative capacity is still observed indicating unambiguously a decomposition reaction either of the electrolyte or of the electrode material. Since we have measured the stability of the electrolyte up to 4.5V, we conclude that the pseudo-plateau observed at 4.07V is due to the oxidative degradation of the  $\text{LiMoN}_2$  electrode material. This is consistent with the blue color of the electrolyte that is observed upon opening the cell, indicative of the presence of  $\text{Mo}^{x+}$  species in solution.

To determine the origin of the pseudo-plateau at 3.73V, cell 2 was charged at a higher scan rate than cell 1, but to a lower charging cut-off voltage (4.1V) in order to prevent the decomposition reaction. A single pseudo-plateau located at an average of 3.8V and corresponding to a 110 mAh/g capacity is observed. This plateau is identical to that observed for cell 1 at 3.73V. The higher voltage observed for the higher scan rate used to cycle the cell is a further indication of the very slow electrochemical process. The plateau corresponds to the deintercalation of lithium from the layered structure as suggested by the X-ray powder pattern recorded at the

end of the charge. On discharge, the voltage of the cell drops sharply to 1.5V and then smoothly to 0.02V so that a capacity of 255 mAh/g is measured. Because the "reduction" reaction occurs at an average voltage of 0.4V (far from the voltage of the deintercalation reaction), it is unlikely that this capacity is due to the insertion of lithium into the structure. At this very low voltage, a likely possibility could be the reductive degradation of the material. This is consistent with the observation that on the second charge, after being discharged to 0.02V, the voltage-composition curve of the cell does not trace back the first charge but is shifted to a higher voltage so that there is a pseudo-plateau located at 4.05V instead of 3.8V as in the first charge. However, the nature of the pseudo-plateau at 4.05V is quite different than that at 3.8V that corresponds to lithium deintercalation, but rather similar to the decomposition plateau observed for cell 1 at 4.05V. When this cell is maintained at a charge of 4.05V, an oxidative capacity is still observed on discharge which is characteristic of the decomposition of the electrode material.

A possible scenario to describe the behavior of the  $\text{LiMoN}_2/\text{Li}$  cell is that upon charging to 4.1V, the starting  $\text{LiMoN}_2$  phase (denoted A) is transformed to a lithium poor phase (B). Upon further charging, the B phase decomposes to a C phase. Therefore, for voltages greater than 4.1V our electrode consists of a mixture of the phases B and C. The discharge of the cell from 4.1V results in another phase (D) so that when the cell reached 0.02V the electrode is a mixture of the B and D phases (it takes at least five electrons to reduce the B phase completely), then upon recharge one reaches a plateau at 4.1V that again corresponds to a decomposition of the B phase into the C phase.

## Discussion

The ideal structure of  $\text{LiMoN}_2$  is composed of stacked hexagonal close-packed sheets of nitrogen with the molybdenum in trigonal prismatic coordination between nitrogen sheets and lithium in octahedral coordination. The X-ray/neutron diffraction data unequivocally shows that the molybdenum is in trigonal prismatic coordination in the predominantly molybdenum layers as predicted for  $d^1$  transition metals in layered dichalcogenide compounds<sup>32</sup> and the lithium is in octahedral coordination in the predominantly lithium layers. However, the data indicates that there are on the order of 16% anti-site defects between the lithium and molybdenum metal layers. The defect concentration appears to be unchanged when  $\text{LiMoN}_2$  is annealed at 300°C.

The N-N distance of 2.8672 Å is the shortest of any binary or ternary nitride known; for example,  $\text{Li}_3\text{N}$  (3.65 Å),  $\text{TiN}$  (3.00 Å)<sup>33</sup> or  $\text{Ca}_3\text{CrN}_3$  (3.01 Å), indicating a significant amount of covalency in  $\text{LiMoN}_2$ .

In contrast to the structure of  $\text{LiMoN}_2$ ,  $\text{LiMoO}_2$  crystallizes in two different structures. The low temperature form, which is prepared by intercalating lithium into  $\text{MoO}_2$ ,<sup>34</sup> has a distorted rutile structure and crystallizes in the space group  $P2_1/c$ . The high temperature form, prepared by reacting  $\text{Li}_2\text{MoO}_4$  with molybdenum metal at 900°C, has a hexagonal layered structure ( $R-3m$ ).<sup>35</sup> In both structural forms, the molybdenum ( $d^3$ ) and lithium atoms are in octahedral holes.

The molybdenum in  $\text{LiMoN}_2$  contains one unpaired d electron which

leads one to predict that this compound should exhibit metallic behavior as in for example  $2H\text{-TaS}_2$  or  $2H\text{-NbSe}_2$ .<sup>32</sup> We have found supporting evidence for this: black in color, Pauli-paramagnetic behavior and a resistivity less than  $2 \times 10^{-3} \Omega \cdot \text{cm}$ .

The asymmetric peaks (Fig. 8) of the deintercalated  $\text{LiMoN}_2$  are likely due to inhomogeneous removal of the lithium: some particles contain more lithium than others or the region near particle surfaces contain less lithium than the middle of the particles. It seems reasonable that this could be quite sensitive to the particle size distribution and to the actual diffusion rate, or the possibility that  $\text{Li}_{1-x}\text{MoN}_2$  may not form a continuous single phase for all  $x$ .

None of the chemical oxidizing agents were able to completely deintercalate the lithium. This may be due in part to a lower lithium diffusion rate at low lithium content, the 0.16Li in the molybdenum layer may be much less mobile than the lithium in the the lithium rich layer, or the potential needed to remove more and more lithium exceeds the oxidizing power of the deintercalating agents being used. This latter possibility is supported by the analytical data showing that more lithium can be deintercalated by  $\text{NOBF}_4$  (+4.7 V vs.  $\text{Li} / \text{Li}^+$ ) than by DDQ (+4.1 V vs.  $\text{Li} / \text{Li}^+$ ). Unfortunately, good PES data was not consistently obtained for the deintercalation products that resulted from using  $\text{NO}_2\text{BF}_4$  (+5.1 V vs.  $\text{Li} / \text{Li}^+$ ). The lithium can be reinserted at room temperature with *n*-butyllithium if the oxidizing gases ( $\text{NO}$  and  $\text{NO}_2$ ) are swept away.

From the electrochemical data, one can conclude that 0.6 Li can be removed from the structure by charging the cell to 4.1V which is in reasonable agreement with the chemical deintercalation data. Attempts to remove more than 0.6 Li resulted in an oxidative decomposition of the

$\text{LiMoN}_2$  phase. This electrochemical process is not reversible since attempts to reinsert lithium electrochemically have been unsuccessful. It is unusual that reintercalation cannot be accomplished electrochemically while chemically it can be. If it is assumed that some oxidative degradation occurs in both methods of deintercalation, it is possible that the degradation product is soluble in refluxing acetonitrile, effectively cleaning the particle surfaces making it possible for reintercalation. However, in the electrochemical case the particles may remain coated making it difficult for reintercalation thus requiring lower potentials for insertion and eventually reductive degradation.

The electrochemical properties of a compound are usually directly related to their structure. The neutron diffraction data indicates the presence of anti-site defects and it is well known<sup>24</sup> that the presence of 3d metal ions within the lithium layers slow the kinetics of the intercalation/deintercalation chemistry considerably. It is possible that as lithium is being removed from the structure the anti-site defect concentration is increased, blocking the lithium diffusion paths and making subsequent lithium intercalation/deintercalation more difficult or even impossible.<sup>36,37</sup> This may also be a source of irreversibility in the electrochemical reactions.

## Conclusion

We have synthesized a new ternary nitride,  $\text{LiMoN}_2$  from two different precursors and ammonia gas. The resistivity and the Pauli-

paramagnetism indicate metallic behavior. It has a layered structure and the lithium can be deintercalated with several different oxidizing agents, as well as in an electrochemical cell; reintercalation is accomplished using n-butyllithium.

### **Acknowledgments**

We are grateful to the Office of Naval Research for its generous support of our nitride work and the Department of Education Fellowship supporting SHE.

We are also grateful to: Mike Rutzke in the Department of Fruit and Vegetables at Cornell University for assistance in the FES analysis, Daccai Xie at the H4S High Flux Beam Reactor at BNL for collecting the neutron diffraction data and Joe Hriljac for the synchrotron X-ray diffraction data collection on beamline X-7A at NSLS supported by the Division of Materials Science (DOE) under contract DE-AC02-76CH0001 to D. E. Cox.

- (1) Gudat, A.; Rabenau, A.; Bronger, W. and Ruschewitz, U. *J. Less - Comm. Met.* **1990**, *161*, 31.
- (2) Gudat, A.; Haag, S.; Kniep, R. and Rabenau, A. *Z. Naturforsch.* **1990**, *45b*, 111.
- (3) Juza, V. A.; Gieren, W. and Haug, J. *Z. Anorg. Allg. Chem.* **1959**, *300*, 61.
- (4) Chern, M. Y. and DiSalvo, F. J. *J. Solid State Chem.* **1990**, *88*, 459.
- (5) Gudat, A.; Haag, S.; Kniep, R. and Rabenau, A. *J. Less - Comm. Met.* **1990**, *159*, L29.
- (6) Chern, M. Y.; Vennos, D. A. and DiSalvo, F. J. *J. Solid State Chem.* **1992**, *96*, 415.
- (7) Jacobs, H. and von Pinkowski, E. *J. Less - Comm. Met.* **1989**, *146*, 147.
- (8) Vennos, D. A.; Badding, M. E. and DiSalvo, F. J. *Inorg. Chem.* **1990**, *29*, 4059.
- (9) Cordier, G.; Hohn, P.; Kniep, R. and Rabenau, A. *Z. Anorg. Allg. Chem.*, in press.
- (10) Gudat, A.; Hohn, P.; Kniep, R. and Rabenau, A. *Z. Naturforsch. B*, in press.
- (11) Hohn, P.; Kniep, R. and Rabenau, A. *Z. Kristallog.* in press.
- (12) Hohn, P. et al. *Angew. Chem. Int. Ed. Engl.* **1991**, *30*(no. 7), 831.
- (13) Whittingham, M. S. *Prog. Solid State Chem.* **1978**, *12*, 41.
- (14) Rouxel, J. In *Physics and Chemistry of Compounds with Layered Structures*; Levy, F., Ed.; Reidel Publ.: Dordrecht, Netherlands, 1979; p 201.

- (15) Whittingham, M. S. *J. Electrochem. Soc.* **1976**, *123*, 315.
- (16) Danopoulos, A. A.; Wilkinson, G.; Hursthouse, M. B. and Hussain, B. *Polyhedron* **1989**, *8(24)*, 2947.
- (17) Rauch, P. E. and DiSalvo, F. J. *Inorg. Synth.* in press.
- (18) Murphy, D. W.; Cros, C.; DiSalvo, F. J. and Waszczak, J. V. *Inorg. Chem.* **1977**, *16*, 3027.
- (19) Dye, J. L., Michigan State University, personal communication, 1991.
- (20) Bollman, D. H. *Anal. Chem.* **1972**, *44*, 887.
- (21) Czechowicz, D. G., Los Alamos National Laboratory, personal communication, 1989.
- (22) Chern, M. Y.; Mariani, R. D.; Vennos, D. A. and DiSalvo, F. J. *Rev. Sci. Instrum.* **1990**, *61(6)*, 1733.
- (23) Yvon, K.; Jeitschko, W. and Parthe, E. *J. Appl. Crystallogr.* **1977**, *10*, 73.
- (24) Thomas, M. G. S. R.; David, W. I. F. and Goodenough, J. B. *Mat. Res. Bull.* **1985**, *20*, 1137.
- (25) Larson, A. C. and Von Dreele, R. B., *Generalized Structure Analysis System*, LANCE, MS-H805, Los Alamos National Laboratory, Los Alamos, NM 87545.
- (26) Rabenau, A. and Schulz, H. *J. Less - Comm. Met.* **1976**, *50*, 155.
- (27) Vassiliou, J.; Hornbostel, M.; Ziebarth, R. and DiSalvo, F. J. *J. Solid State Chem.* **1989**, *81*, 208.
- (28) Selwood, P. W. *Magnetochemistry*; Wiley-Interscience: New York, 1979; p 186.
- (29) Wizansky, A. R.; Rauch, P. E. and DiSalvo, F. J. *J. Solid State Chem.* **1989**, *81*, 208.

- (30) Guyomard, D. and Tarascon, J. M. *J. Electrochem. Soc.*, in press.
- (31) Mac Pile Data Acquisition System for Insertion Compounds, CNRS, Grenoble, France.
- (32) Mattheiss, L. F. *Phys. Rev. B* **1973**, *8*, 3719.
- (33) Beattie, H. J. and VerSnyder, F. L. *Trans. Am. Soc. Met.* **1953**, *45*, 397.
- (34) Murphy, D. W.; DiSalvo, F. J.; Carides, J. N. and Waszczak, J. V. *Mat. Res. Bull.* **1978**, *13*, 1395.
- (35) Aleandri, L. E. and McCarley, R. E. *Inorg. Chem.* **1988**, *27*, 1041.
- (36) Murphy, D. W. *NATO Conf. Ser. E.* **1985**, *101*, 181.
- (37) Sandre, E.; Brec, R. and Rouxel, J. *J. Solid State Chem.* **1990**, *88*, 269.

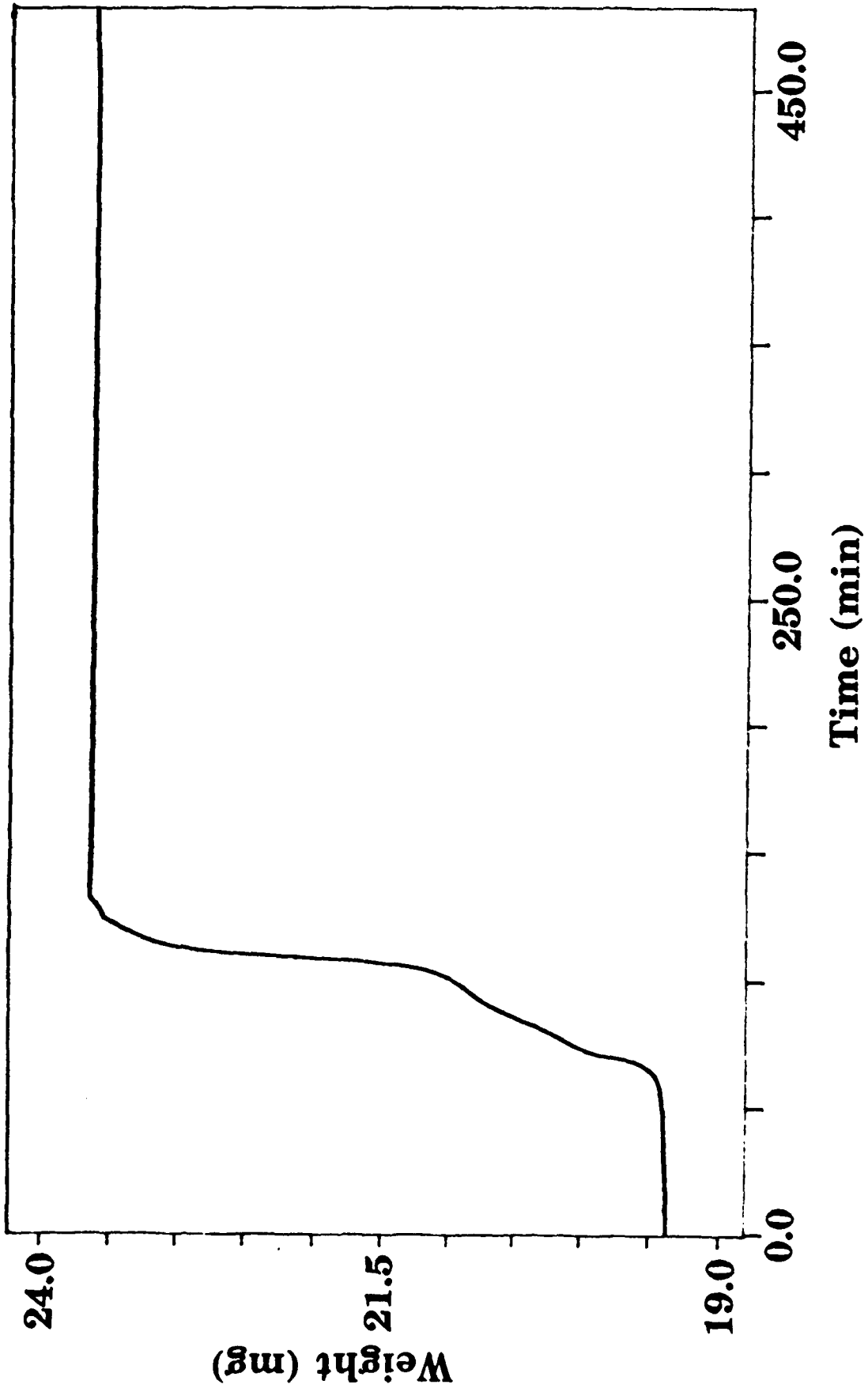


**Table I.** Ideal positional parameters initially proposed for the possible structure of  $\text{LiMoN}_2$ .

**space group  $R\bar{3}$**

atom	site	x	y	z
Mo	3a	0	0	0
Li	3a	0	0	5/6
N(1)	3a	0	0	1/4
N(2)	3a	0	0	5/12

**space group  $R\bar{3}m$**

Mo	3a	0	0	0
Li	3b	0	0	1/2
N	6c	0	0	1/4

**Table II.** The measured intensities and d-spacings for  $\text{LiMoN}_2$  from the preliminary X-ray work, and the calculated intensities and d-spacings for  $\text{LiMoN}_2$  if the Mo is in trigonal prismatic (tp) or octahedral (oct) coordination.

<b>hkl</b>	<b><math>d_{(\text{meas.})}(\text{\AA})</math></b>	<b><math>I_{(\text{meas.})}</math></b>	<b><math>d_{(\text{calc.})}(\text{\AA})</math></b>	<b><math>I_{\text{tp}(\text{calc.})}</math></b>	<b><math>I_{\text{oct}(\text{calc.})}</math></b>
003	5.2495	100	5.2493	100	100
006	2.6311	21.9	2.6247	11.6	11.6
101	2.4522	35.4	2.4576	41.2	43.5
102	2.3683	20.3	2.3725	37.1	26.8
104	2.1012	16.7	2.1033	33.2	52.6
105	1.9523	23.6	1.9524	32.7	21.9
009	1.7541	2.18	1.7498	5.16	5.16
107	1.6696	10.9	1.6687	19.5	13.3
108	1.5465	4.22	1.5438	12.2	18.6
110	1.4350	8.64	1.4365	14.5	14.5
113	1.3827	4.03	1.3856	14.4	14.4
1010	1.3333	2.25	1.3307	6.15	5.10
0012	1.3153	2.21	1.3123	3.54	3.54
116	1.2590	4.52	1.2601	8.70	8.70
1011	1.2411	2.78	1.2409	5.10	5.12
201	1.2396	2.77	1.2402	5.09	5.11
202	1.2288	0.0	1.2288	4.83	4.05
204	1.1862	1.31	1.1862	5.23	7.71
205	1.1559	2.07	1.1571	5.89	4.21
119	1.0908	1.84	1.1103	7.62	7.62
1013	1.0890	2.02	1.0892	3.65	3.66
207	1.0878	1.98	1.0887	5.07	3.66
208	1.0516	0.0	1.0516	3.96	5.74
0015	1.0499	0.0	1.0499	1.14	1.14
1014	1.0250	0.0	1.0250	3.21	2.74
2010	0.9737	1.44	0.9762	3.07	2.62
1112	0.9698	2.81	0.9689	10.4	10.4
2011	0.9382	1.93	0.9390	3.12	3.15
211	0.9371	2.27	0.9387	6.24	6.30
122	0.9345	1.38	0.9338	6.12	5.12
1016	0.9152	0.0	0.9152	3.67	5.23
214	0.9147	0.0	0.9147	7.34	10.48
125	0.8999	1.50	0.9011	8.84	6.54

**Table III.** Refined positional and thermal parameters from the joint X-ray<sup>†</sup> and neutron<sup>§</sup> refinements of LiMoN<sub>2</sub> (*R*3, *Z*=3)\*.

Atom	site	x	y	z	$U_{\text{iso}}(\text{\AA}^2 \times 100)$
Mo(1) <sup>Δ</sup>	3a	0.0	0.0	0.0	0.6(1)
Li(1) <sup>Δ</sup>	3a	0.0	0.0	0.8290(18)	5.7(8)
N(1)	3a	0.0	0.0	0.2520(4)	2.5(1)
N(2)	3a	0.0	0.0	0.4141(4)	1.6(1)

<sup>†</sup> refined cell parameters (Å) for the X-ray case:  $a=2.8674(3)$ ,  $c=15.801(2)$ ;  $R_{\text{wp}}=0.185$ ,  $R_{\text{p}}=0.144$ ,  $R_{\text{N}}=0.057$ .

<sup>§</sup> refined cell parameters (Å) for the neutron case:  $a=2.8672(3)$ ,  $c=15.813(3)$ ;  $R_{\text{wp}}=0.092$ ,  $R_{\text{p}}=0.074$ ,  $R_{\text{N}}=0.057$ .

\* overall powder statistics for both refinements:  $R_{\text{wp}}=0.128$ ,  $R_{\text{p}}=0.079$ ,  $\chi^2=2.01$ .

<sup>Δ</sup> partially occupied sites: the site designated Mo(1) has composition (Mo<sub>0.840(5)</sub> Li<sub>0.160(5)</sub>) and the Li(1) site has the constrained composition (Mo<sub>0.160(5)</sub> Li<sub>0.840(5)</sub>), thereby ensuring the overall stoichiometry for the phase LiMoN<sub>2</sub>.

**Table IV.** Selected interatomic distances (Å) and angles (°) for LiMoN<sub>2</sub>.

<u>Bond Distances</u>	
Mo(1)–N(1) x 3	2.095(4)
Mo(1)–N(2) x 3	2.091(4)
Li(1)–N(1) x 3	2.179(18)
Li(1)–N(2) x 3	2.098(17)

<u>Angles</u>	
N(1)–Mo(1)–N(1) x 6	86.34(9)
N(1)–Mo(1)–N(2) x 3	75.45(9)
N(1)–Mo(1)–N(2) x 6	133.41(3)
N(1)–Li(1)–N(1) x 3	82.3(8)
N(1)–Li(1)–N(2) x 6	95.72(8)
N(1)–Li(1)–N(2) x 3	177.3(9)
N(2)–Li(1)–N(2) x 3	86.2(9)

**Table V.** The observed d-spacings for  $\text{LiMoN}_2$  and  $\text{LiMoN}_2$  deintercalated with  $\text{NOBF}_4$  as determined by X-ray powder diffraction.

	$\text{LiMoN}_2$	$\text{Li}_x\text{MoN}_2(x=0.36)$
h k l	d(Å)	d(Å)
003	5.250	5.167
006	2.631	2.586
101	2.452	2.448
102	2.368	2.361
		2.239*
		2.185*
104	2.101	2.090
		2.032*
		2.015*
105	1.952	1.939

\* refers to second phase peaks

## Figure Captions

**Figure 1.** TGA of  $\text{LiMoN}_2$  in air:  $30^\circ\text{C}$  to  $100^\circ\text{C}$  at  $2^\circ\text{C}/\text{min}$ ;  $100^\circ\text{C}$  to  $700^\circ\text{C}$  at  $5^\circ\text{C}/\text{min}$ ;  $700^\circ\text{C}$  for 300min;  $700^\circ\text{C}$  to  $30^\circ\text{C}$  at  $25^\circ\text{C}/\text{min}$ .

**Figure 2.** X-ray powder diffraction pattern of  $\text{LiMoN}_2$ .

**Figure 3.** The neutron diffraction data for  $\text{LiMoN}_2$  collected at 293K at the steady state source at Brookhaven National Lab (BNL). Points shown by (+) represent observed data. The continuous lines through the sets of points are the calculated profiles from refinements given in Table III. The tic marks below the data indicate the positions of the allowed reflections for both  $\text{LiMoN}_2$  (bottom set) and  $\text{Li}_2\text{O}$  (top set). The lower curve represents the difference between observed and calculated profiles. Gaps in the pattern are regions containing peaks arising from impurities and were excluded from the refinement.

**Figure 4.** The X-ray data for  $\text{LiMoN}_2$  collected at 300K at the National Synchrotron Light Source (NSLS) at BNL. Points shown as (+) represent observed data. The continuous lines through the sets of points are the calculated profiles from the refinements given in Table III. The set of tic marks below the data indicate the positions of the allowed reflections. Gaps in the pattern are regions containing peaks arising from impurities and were excluded from the refinement. The lower curve represents the difference between observed and calculated profiles.

**Figure 5.** Part of the structure of  $\text{LiMoN}_2$  emphasizing the coordination of the site between the  $\text{MoN}_2$  layers that is predominantly occupied by Li (large circles). The (001) face of the unit cell is outlined.

**Figure 6.** Temperature dependent susceptibility of  $\text{LiMoN}_2$ .

**Figure 7.** Approximate potentials (vs. standard hydrogen electrode) of the oxidizing agents, in dry acetonitrile, used for the deintercalation of  $\text{LiMoN}_2$  (adapted from ref. 27).

**Figure 8.** The X-ray powder pattern of  $\text{Li}_{0.36}\text{MoN}_2$  (deintercalated with  $\text{NOBF}_4$ ) superimposed on the powder pattern for  $\text{LiMoN}_2$ .  $\text{Li}_{0.36}\text{MoN}_2$  peaks are denoted by an x and second phase peaks (introduced by the deintercalation reaction) by an o.

**Figure 9.** Voltage-composition curve for cell 1. It was charged to 4.2V at 2mV/hr and then discharged to 2.7V. Phase A is  $\text{LiMoN}_2$ , phase B is a lithium poor phase ( $\text{Li}_{1-x}\text{MoN}_2$ ), phase C results from the oxidative decomposition of B.

**Figure 10.** Voltage-composition curve for cell 2. It was charged to 4.1V at 10mV/hr and then cycled between 4.1V and 0.02V for one cycle. Phases A, B and C are the same as in Figure 9; phase D results from the reductive decomposition of B.

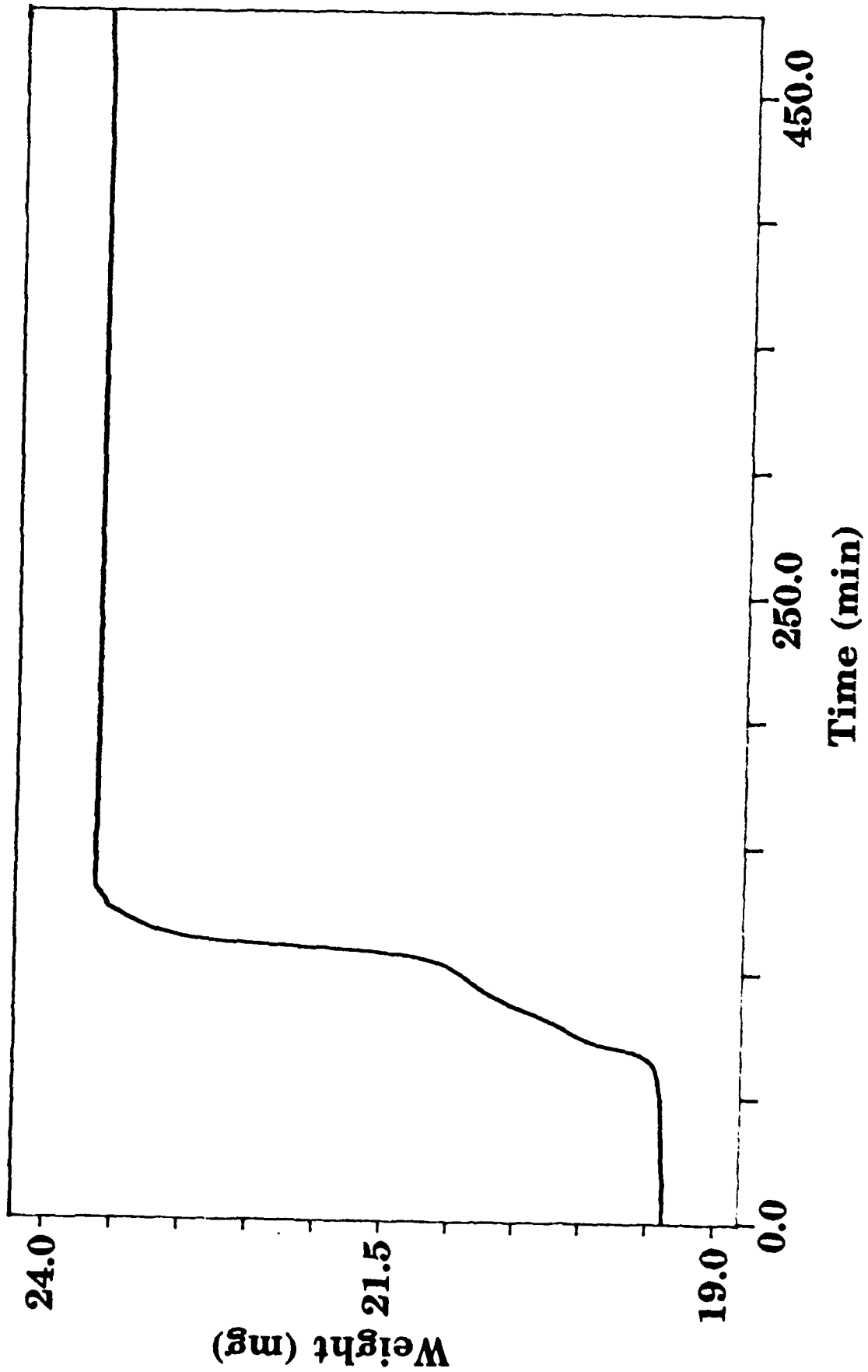


Fig 1

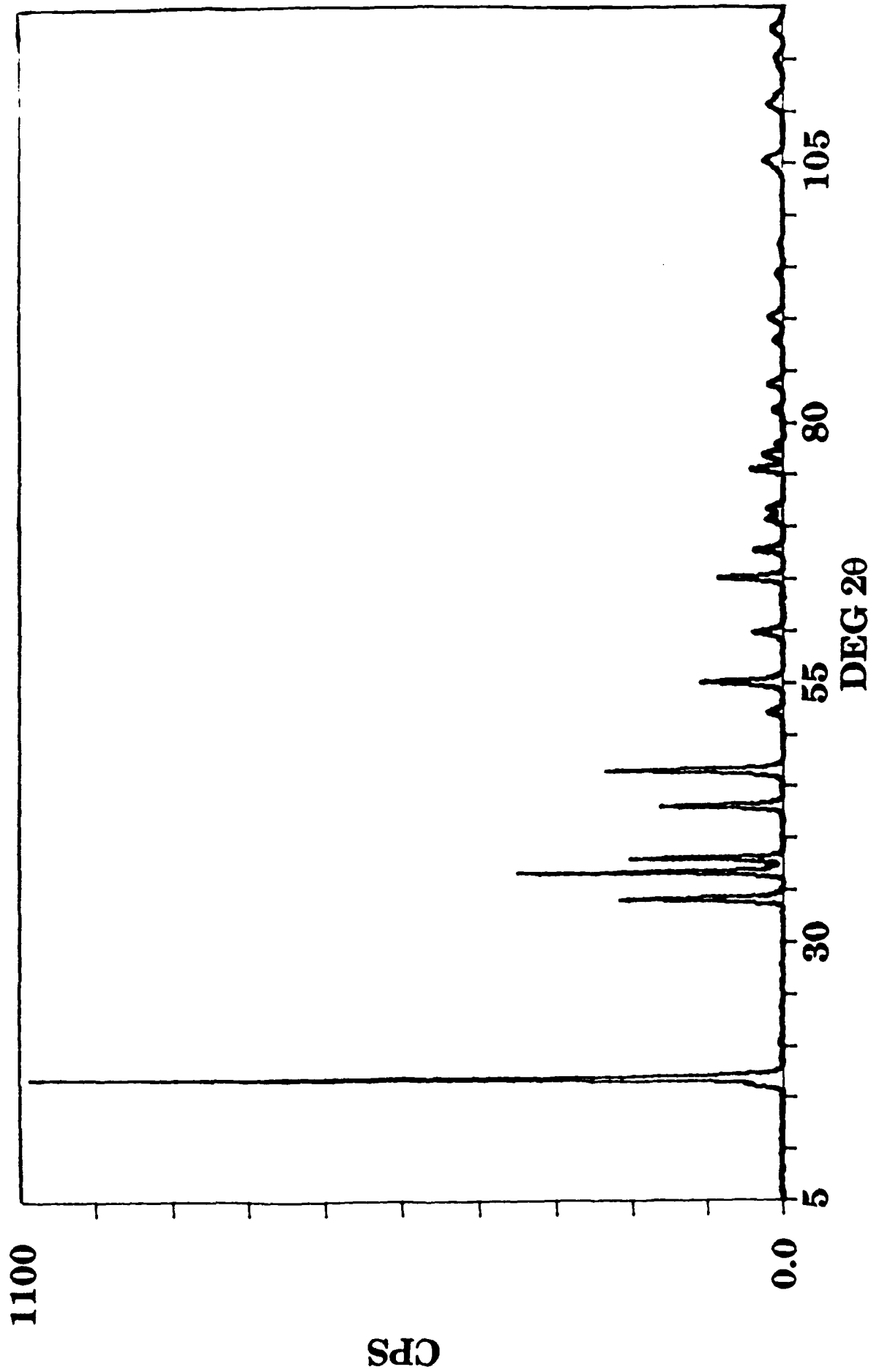


Fig 2

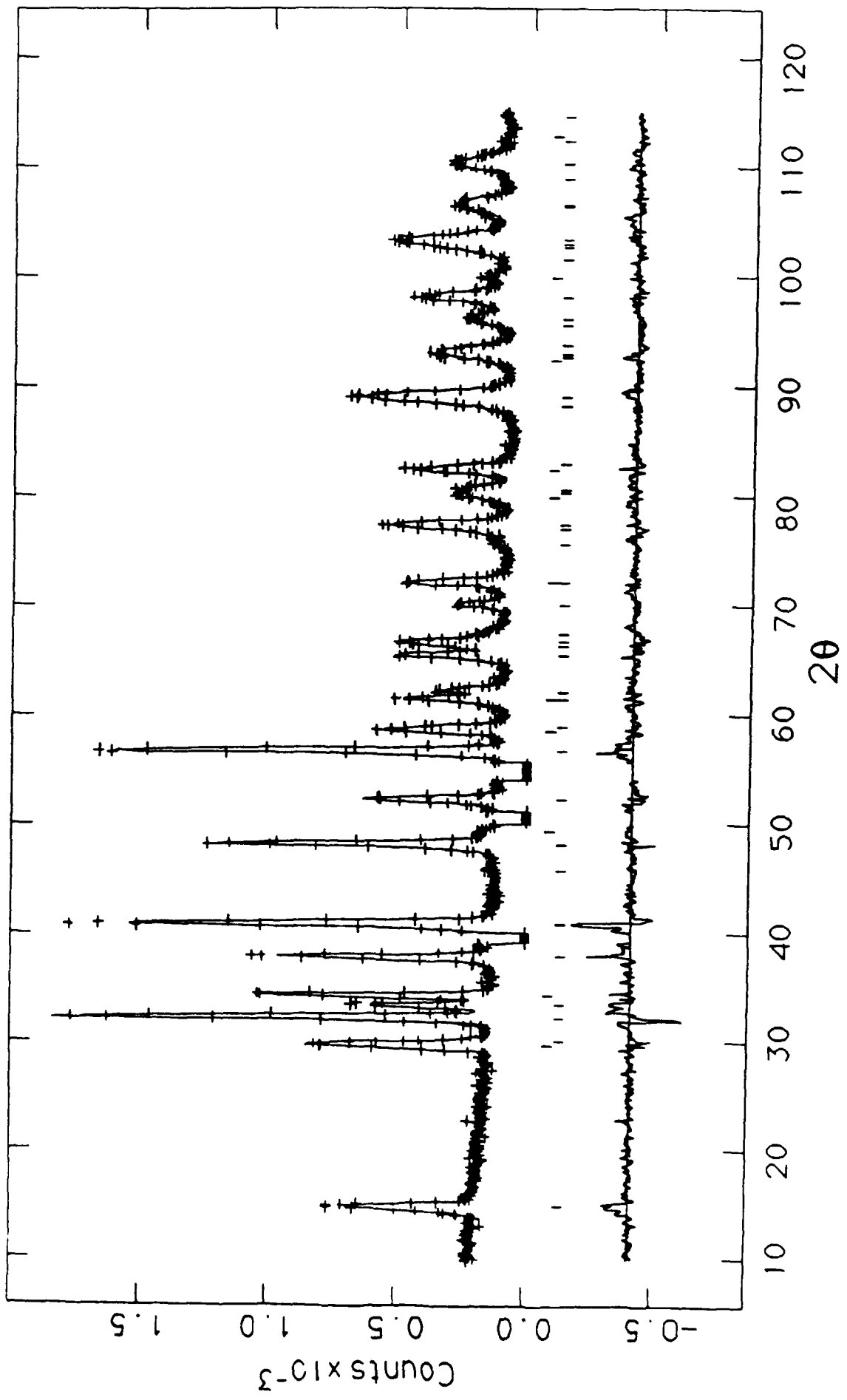


Fig 3

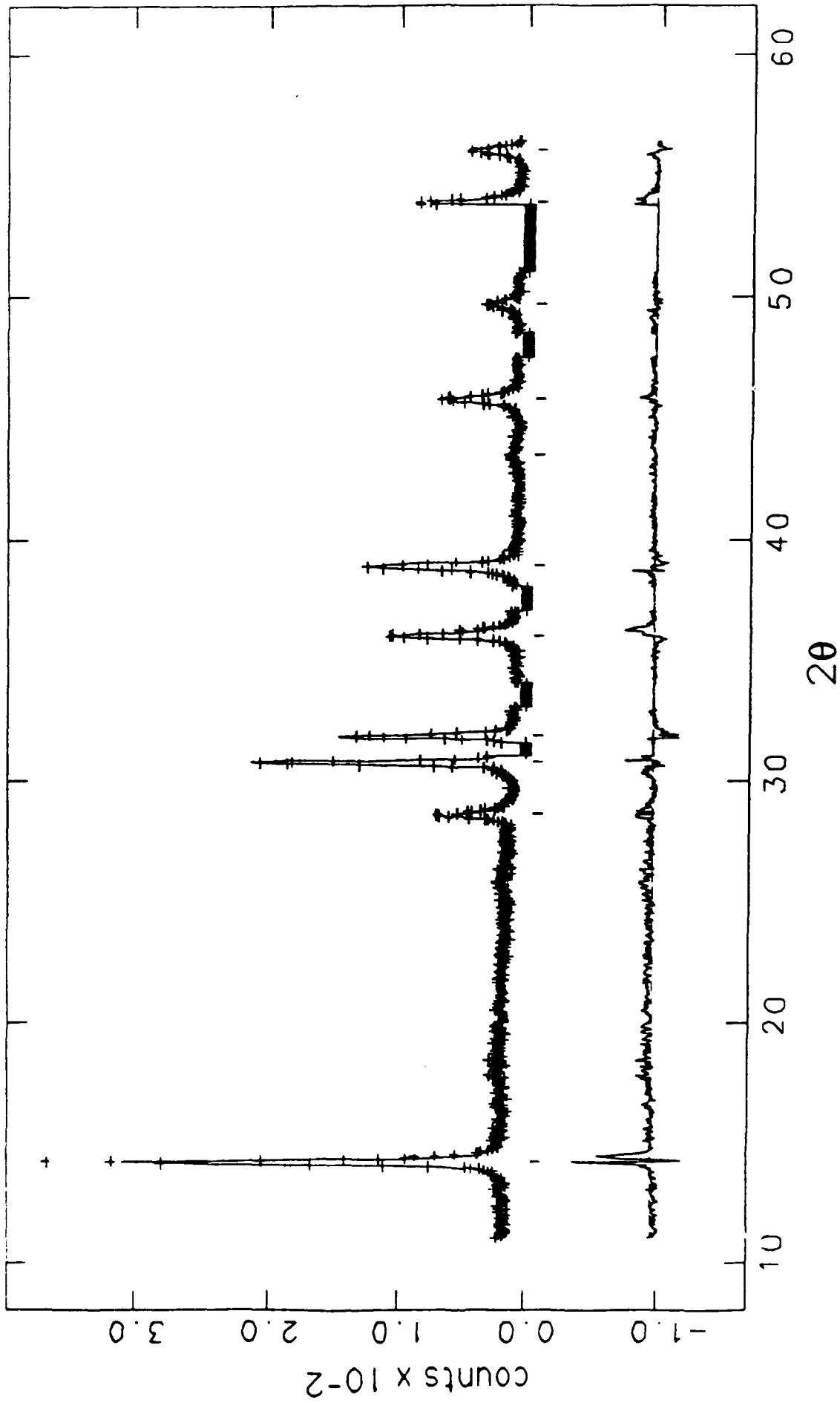


Fig 4

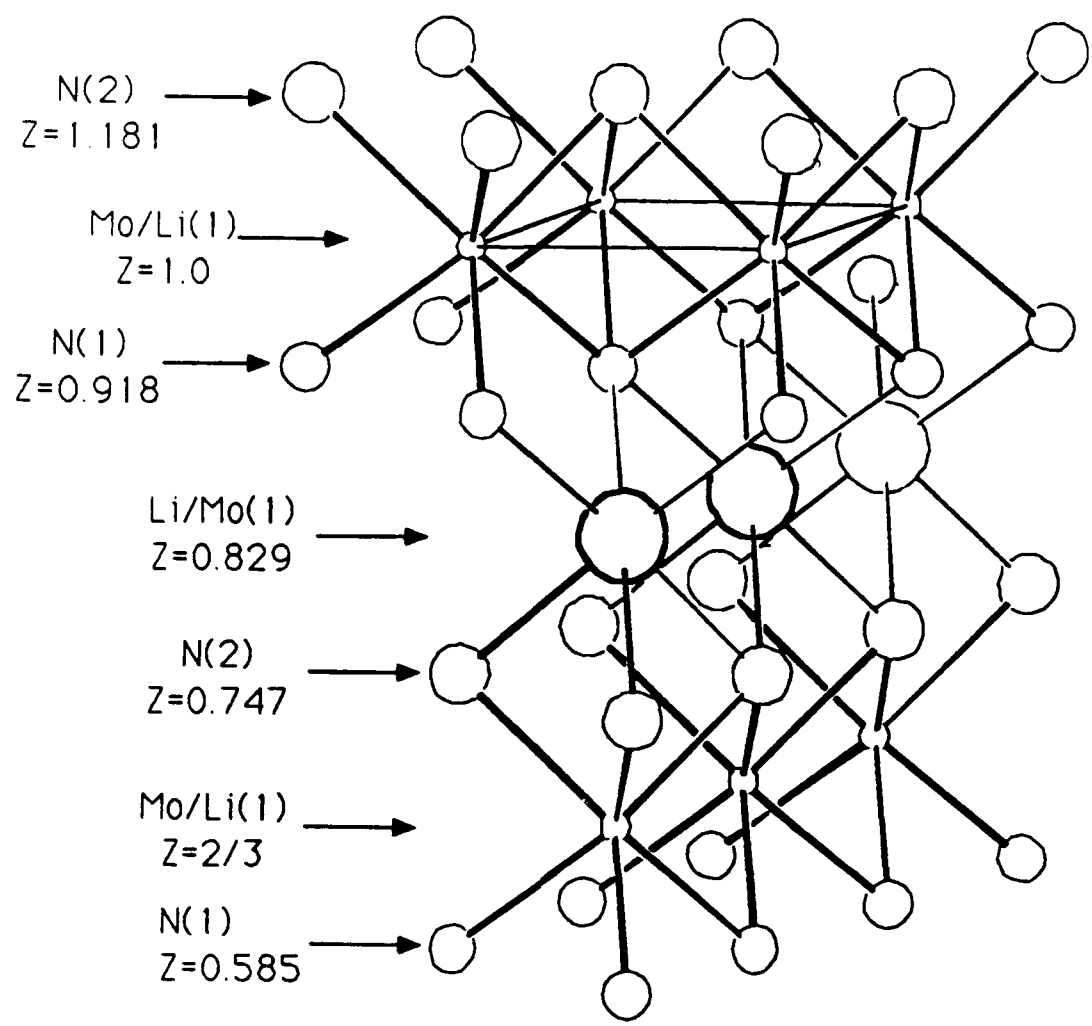


Fig 5

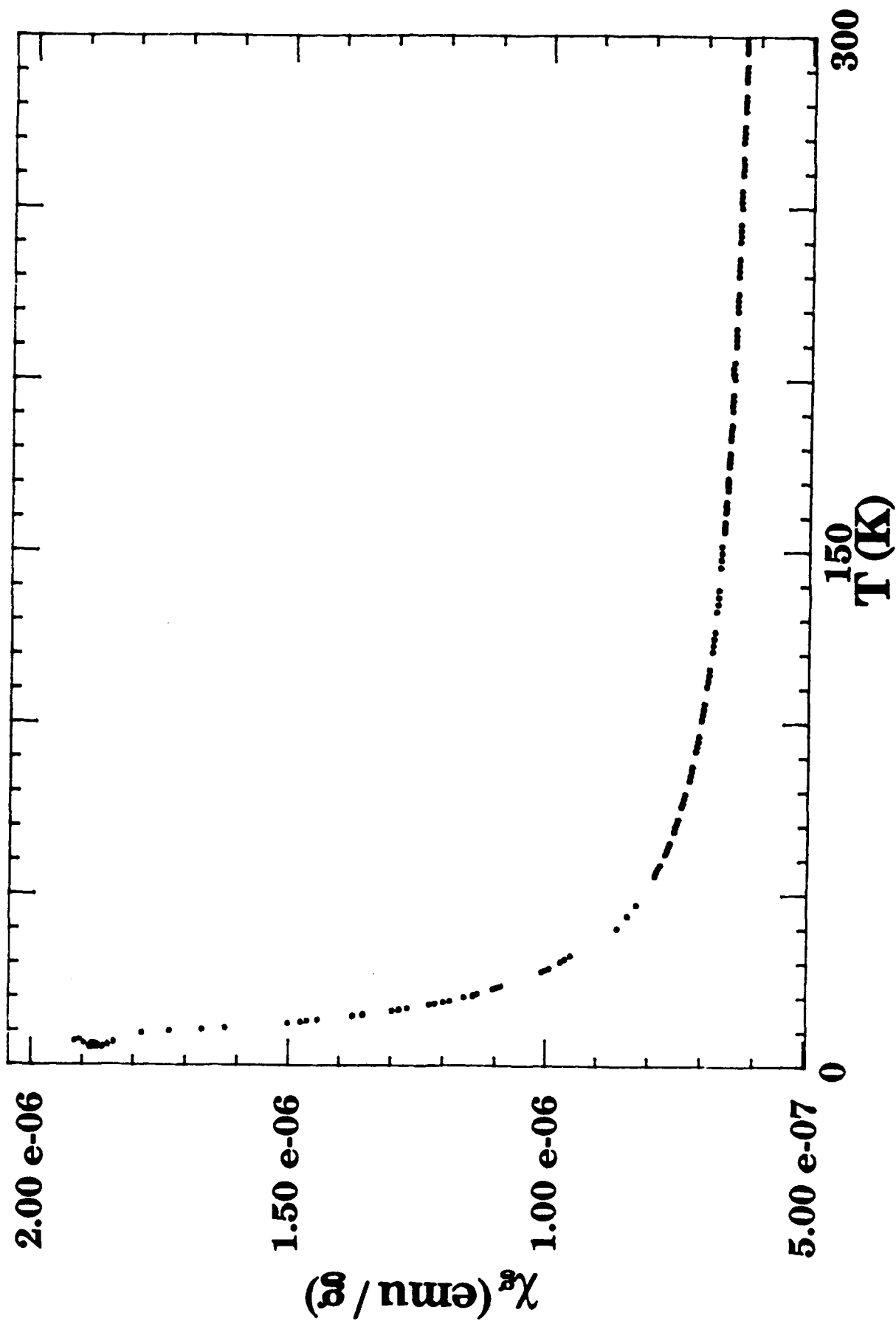


Fig 6

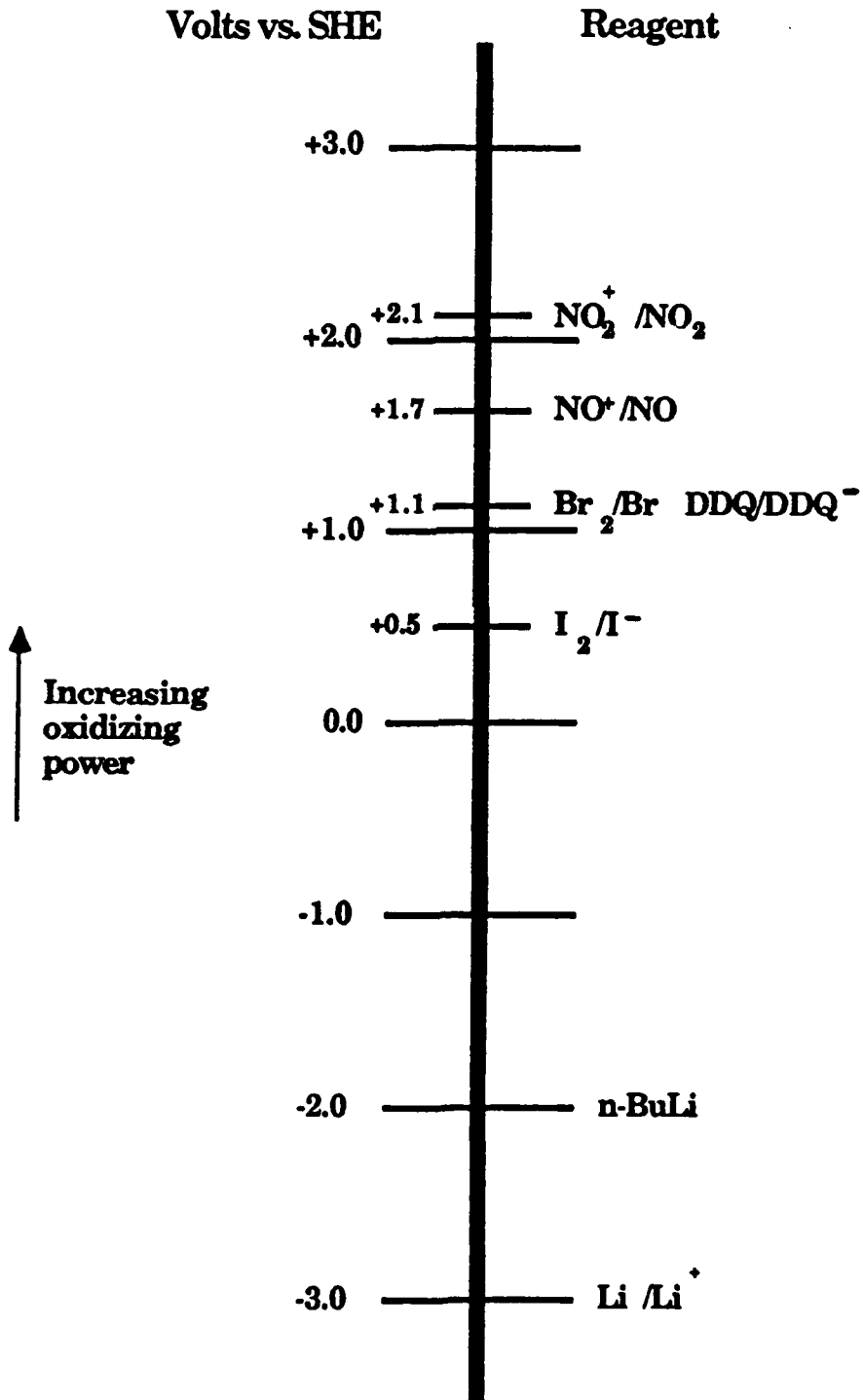


Fig 7

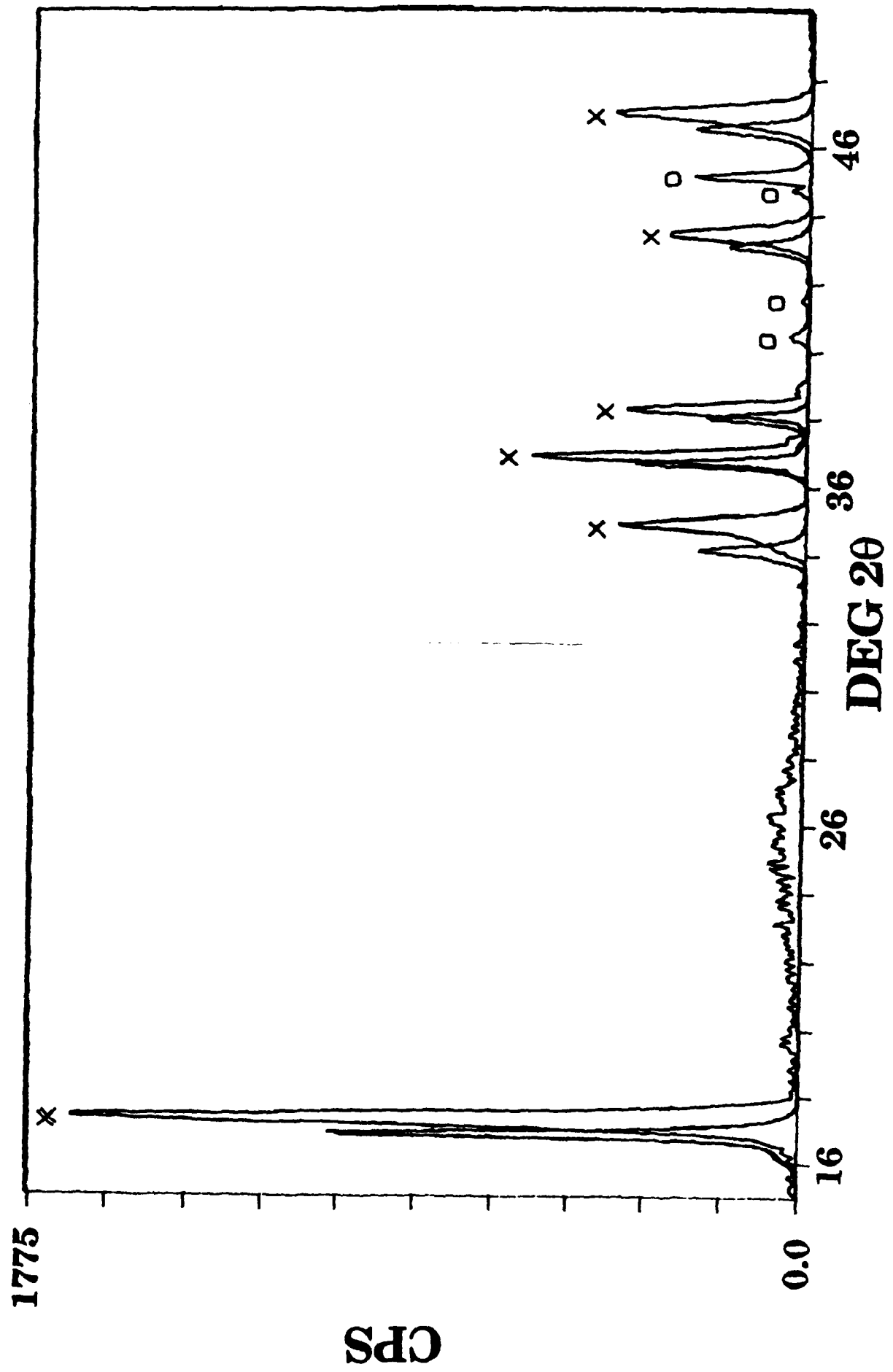


Fig 8

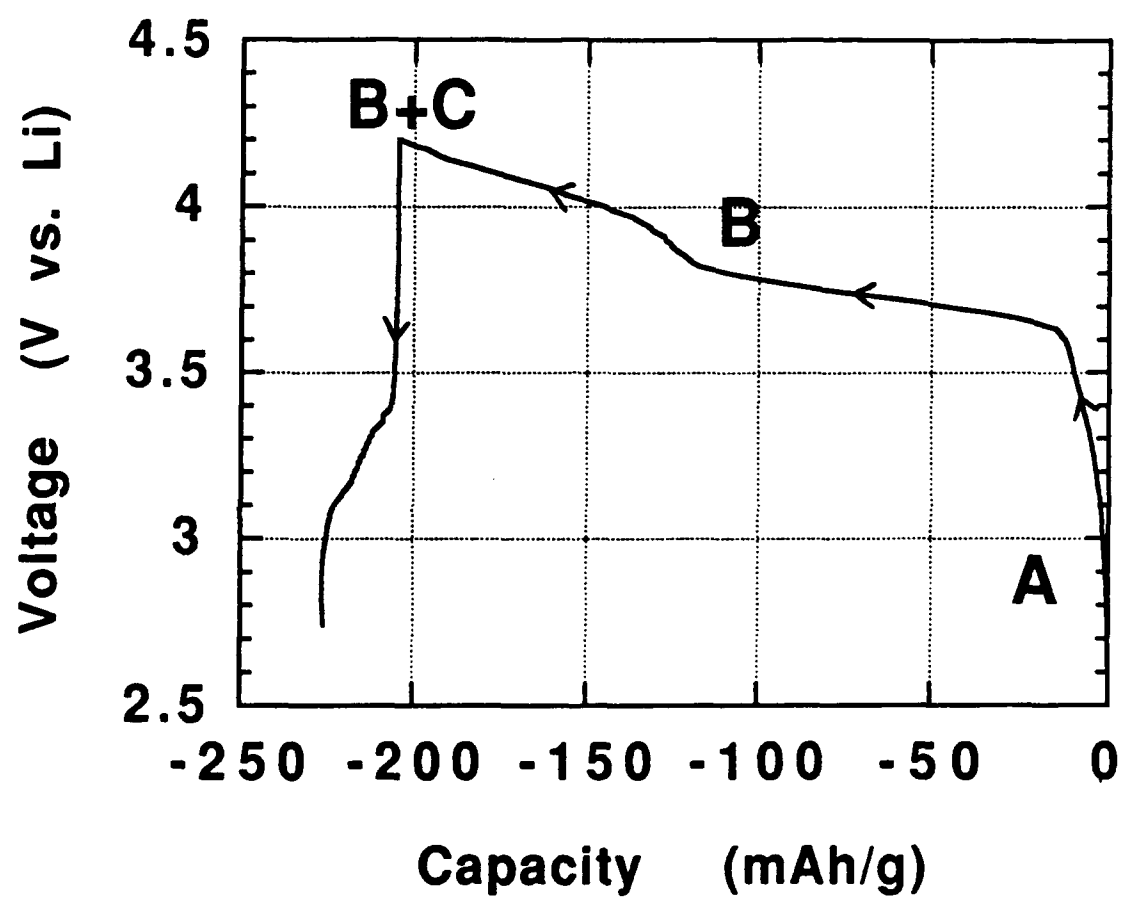


Fig 9

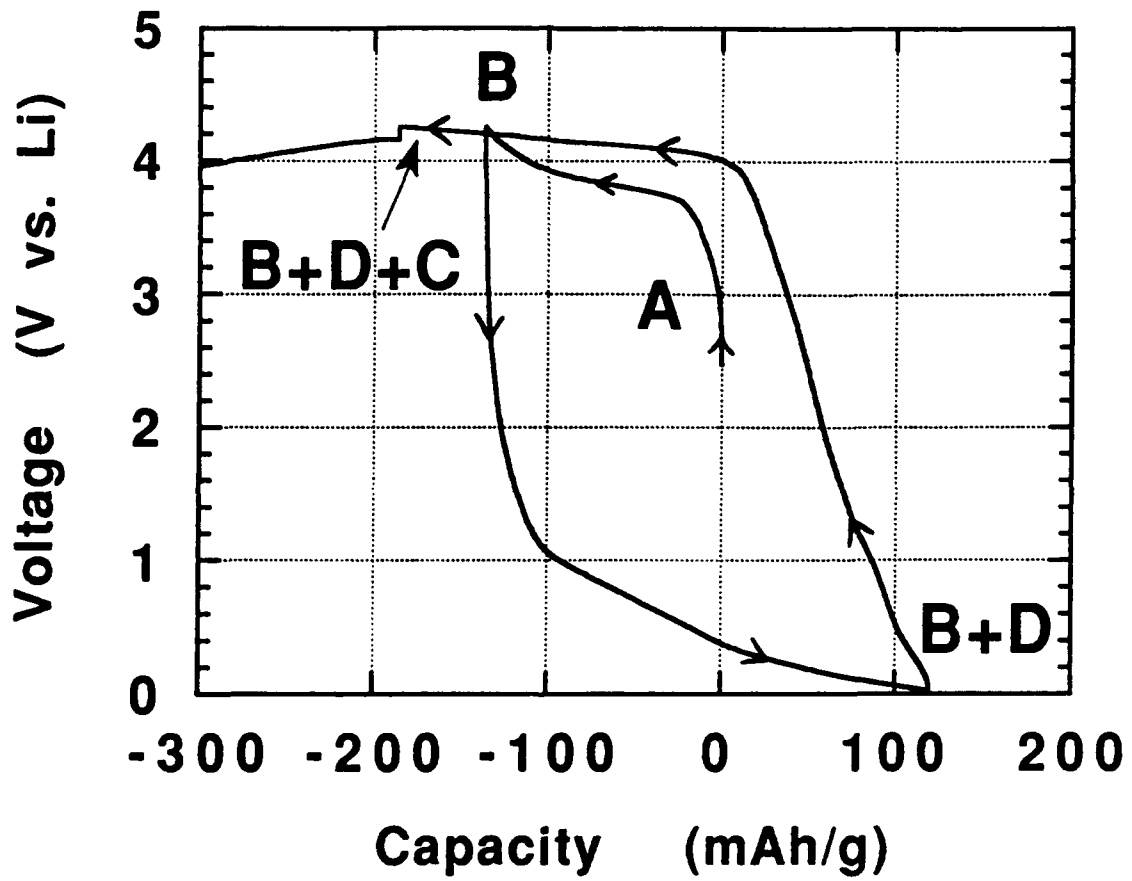


Fig 10

TECHNICAL REPORT DISTRIBUTION LIST - GENERAL

Office of Naval Research (2)  
Chemistry Division, Code 1113  
800 North Quincy Street  
Arlington, Virginia 22217-5000

Dr. Richard W. Drisko (1)  
Naval Civil Engineering  
Laboratory  
Code L52  
Port Hueneme, CA 93043

Dr. James S. Murday (1)  
Chemistry Division, Code 6100  
Naval Research Laboratory  
Washington, D.C. 20375-5000

Dr. Harold H. Singerman (1)  
David Taylor Research Center  
Code 283  
Annapolis, MD 21402-5067

Dr. Robert Green, Director (1)  
Chemistry Division, Code 385  
Naval Weapons Center  
China Lake, CA 93555-6001

Chief of Naval Research (1)  
Special Assistant for Marine  
Corps Matters  
Code OOMC  
800 North Quincy Street  
Arlington, VA 22217-5000

Dr. Eugene C. Fischer (1)  
Code 2840  
David Taylor Research Center  
Annapolis, MD 21402-5067

Defense Technical Information  
Center (2)  
Building 5, Cameron Station  
Alexandria, VA 22314

Dr. Elek Lindner (1)  
Naval Ocean Systems Center  
Code 52  
San Diego, CA 92152-5000

Commanding Officer (1)  
Naval Weapons Support Center  
Dr. Bernard E. Doua  
Crane, Indiana 47522-5050

\* Number of copies to forward